INTERNATIONAL JOURNAL FOR NUMERICAL METHODS IN ENGINEERING
Int. J. Numer. Meth. Engng 2003; **57**:2221–2240 (DOI: 10.1002/nme.849)

New crack-tip elements for XFEM and applications to cohesive cracks

Goangseup Zi and Ted Belytschko*,†

Department of Mechanical Engineering, Northwestern University, 2145 Sheridan Road, Evanston, IL 60208-3111, U.S.A.

SUMMARY

An extended finite element method scheme for a static cohesive crack is developed with a new formulation for elements containing crack tips. This method can treat arbitrary cracks independent of the mesh and crack growth without remeshing. All cracked elements are enriched by the sign function so that no blending of the local partition of unity is required. This method is able to treat the entire crack with only one type of enrichment function, including the elements containing the crack tip. This scheme is applied to linear 3-node triangular elements and quadratic 6-node triangular elements. To ensure smooth crack closing of the cohesive crack, the stress projection normal to the crack tip is imposed to be equal to the material strength. The equilibrium equation and the traction condition are solved by the Newton–Raphson method to obtain the nodal displacements and the external load simultaneously. The results obtained by the new extended finite element method are compared to reference solutions and show excellent agreement. Copyright © 2003 John Wiley & Sons, Ltd.

KEY WORDS: fracture; finite elements; crack growth; cohesive crack

1. INTRODUCTION

One of the most awkward problems encountered in the analyses of crack growth is that remeshing is required near the crack tip as the crack grows. Such remeshing is not only burdensome but it requires projection of variables between the different meshes and causes difficulties during post-processing, for example, when a variable at a spatial point is monitored. This difficulty may be avoided by meshless methods, such as the element-free Galerkin method (EFGM) [1], or the extended finite element method (XFEM) [2]. The latter is especially well-suited to the structure of existing commercial finite element codes.

*Correspondence to: Ted Belytschko, Department of Mechanical Engineering, Northwestern University, 2145 Sheridan Road, Evanston, IL 60208-3111, U.S.A.
†E-mail: tedbelytschko@northwestern.edu

Contract/grant sponsor: Office of Naval Research

Received 3 January 2003
Revised 14 February 2003
Accepted 10 March 2003

The key idea of the extended finite element method (XFEM) is that part of the displacement field is approximated by a discontinuous displacement enrichment [2] based on a local partition of unity [3, 4]. The displacement field thus is approximated by the sum of the regular displacement field, which is the displacement without any discontinuities, and the enrichment displacement field, which is the additional displacement that models the discontinuities. A good engineering explanation of the nodal enrichment can be found in Moës *et al.* [5].

XFEM was first developed for two-dimensional linear elastic fracture mechanics (LEFM) [2]. A single crack was considered and the near-tip field solutions were used as the nodal enrichment functions. XFEM has subsequently been extended to many applications; step function enrichment [5, 6], crack growth with friction [7], arbitrary branched and intersecting cracks [8], three-dimensional crack propagation [9], material discontinuity problems (strain discontinuity) [10, 11], etc. The method has been successfully applied to fluid mechanics, too [12].

Recently, a second-order XFEM scheme was developed for linear elastic fracture by Stazi *et al.* [13]. But they used a quadratic field only for the continuous displacement field. The enrichment in their work was linear, so the crack opening profile in elements not containing the crack tip is linear. Wells *et al.* [14] have used the extended finite element concept with 6-node triangular elements but limited their enrichment to the case where cracks end at element edges.

In this paper, we develop a new enrichment technique by which curved cracks can be treated with higher order enrichments. The crack tip can be located anywhere within an element. The technique is based on Chen's [15] development for constant strain triangles. In addition, we closely examine the accuracy of these method for the static cohesive crack model.

The cohesive crack model was introduced by Dugdale [16] and Barenblatt [17]. It has been used extensively in non-linear fracture mechanics of quasibrittle materials [18–24], etc. In the cohesive crack model, the stress singularity at the crack tip found in LEFM is cancelled by the stress intensity factor due to the cohesive stress on the crack surfaces in the fracture process zone. The cohesive stress depends on the crack opening displacement in the fracture process zone and, typically, decreases (or softens) as the crack opening displacement increases.

There are other applications of XFEM to the cohesive crack models. Wells and Sluys [25] applied the XFEM concept to the cohesive crack model but limited their enrichment to the case where cracks end at element edges. Moës and Belytschko [21] implemented the XFEM scheme for cohesive cracks in linear triangular elements. In their work, a linear element is enriched by the step function if it is completely cut by a crack, and by the branch function if the crack tip is located inside the element. Their load–deflection responses compare well to experimental results.

In the enrichment developed here, an element containing a crack tip is enriched by the sign of a signed distance function whose gradient is normal to the crack and a polynomial along the crack. We consider polynomials of first and second order but the method is applicable to any order. The contribution of the paper lies in that the branch function used in previous XFEM [21] formulations for cracks is dropped, so that the partition of unity holds in the entire enriched subdomain. Both a first-order scheme and a second-order scheme are developed by this procedure. The scheme can be applied to various non-linear softening laws.

2. ENRICHMENT OF DISPLACEMENT FIELD

For elements completely cut by a crack, the step function has been successfully used in many applications [2, 5, 8, 9, 21, 26]. We will here use the sign function instead of the step function because of its appealing symmetry, but the numerical discretization is identical. The sign function is defined as

$$\operatorname{sign}(x) = \begin{cases} -1 & \text{for } x < 0 \\ +1 & \text{for } x > 0 \end{cases} \tag{1}$$

The sign function enrichment is equivalent to the Heaviside step function enrichment, which is the nomenclature used in preceding works.

If a crack grows element by element, i.e. if the crack tip is always located on an edge of an element, a successful element can be devised by using only the sign function without other enrichment functions [14, 15, 25]. When a crack grows smoothly, the crack tip may be located inside an element. Then we must account for elements partially cut by a crack. This kind of element will be called a tip element. In this case, the sign function cannot be used directly because the sign function does not yield the appropriate displacement field for the tip element.

Branch functions, typically, $r^m \sin \vartheta/2$ where $m = 0.5,\ 1.0.$ etc., have been used for the enrichment of the tip element [2, 10, 13, 21]. For a discussion of the branch function, see Belytschko *et al.* [10]. When branch functions are used in conjunction with step functions, as in Reference [5], the partition of unity property does not hold in the elements surrounding the tip element. The enrichment of those elements is a local partition of unity and it must be blended to the rest of the domain for optimal performance because the branch function does not vanish at the edges of the tip element. Note that the branch function is not a piecewise constant function like the sign function. For a discussion of local partitions of unity and blending, see Chessa *et al.* [4].

In order to avoid the difficulties associated with the branch functions in the tip element, a new enrichment is developed here. This procedure is similar to that given by Chen [15] but it is generalized to quadratic elements in this paper. It can be applied to elements of any order without difficulty.

Consider a crack Γ_c in a two-dimensional body Ω with boundary Γ as shown in Figure 1. We denote by $\mathbf{x}$ the spatial co-ordinates. The crack is described implicitly by the level set function

$$\phi(\mathbf{x}) = 0 \tag{2}$$

and its two end points $\mathbf{x}_I^{\mathrm{cr}}$, $I = 1, 2$. Depending on the cohesive law, a traction $\boldsymbol{\tau}^{\mathrm{c}}$ is applied across the crack surface near the tip.

The displacement field $\mathbf{u}$ of the body can be additively decomposed into a continuous part $\mathbf{u}_{\mathrm{cont}}$ and a discontinuous part $\mathbf{u}_{\mathrm{disc}}$:

$$\mathbf{u}(\mathbf{x}) = \mathbf{u}_{\mathrm{cont}}(\mathbf{x}) + \mathbf{u}_{\mathrm{disc}}(\mathbf{x}) \tag{3}$$

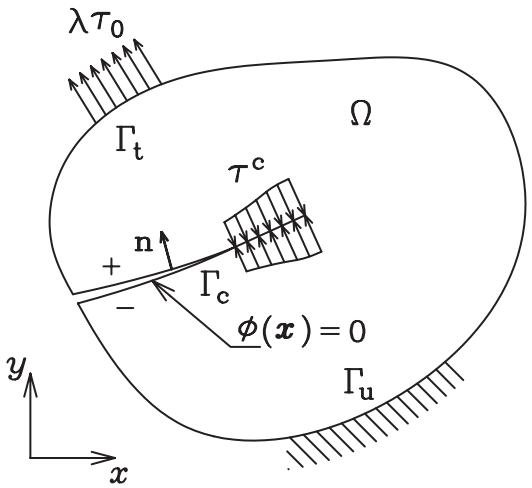

Figure 1. A two-dimensional domain containing a cohesive crack inside the domain.

The discontinuous part of the displacement field is approximated by standard C^0 shape functions $N_I(\mathbf{x})$, so

$$\mathbf{u}_{\text{cont}}(\mathbf{x}) = \sum_{I \in N_{\text{tot}}} N_I(\mathbf{x})\mathbf{u}_I \tag{4}$$

where N_{tot} is the total set of nodes and $\mathbf{u}_I$ are nodal displacements.

If we consider a triangulation on the body Ω as shown in Figure 2, then the discontinuous part of the displacement field can be limited to the elements that contain the crack. We call this subdomain Ω_{enr}. Let N_{enr} be the set of nodes of the elements cut by the crack Γ_c. The discontinuous part of the displacement field can then be written as [2]

$$\mathbf{u}_{\text{disc}}(\mathbf{x}) = \sum_{I \in N_{\text{enr}}} N_I(\mathbf{x})\Psi_I(\mathbf{x})\mathbf{a}_I \tag{5}$$

where $\Psi_I(\mathbf{x})$ are enrichment functions and $\mathbf{a}_I$ are enrichment parameters.

We now discuss how these enrichment functions are constructed. For this purpose, we consider separately elements completely cut by a crack and those containing the crack tip. For elements in Ω_{enr} completely cut by the crack,

$$\Psi_I(\mathbf{x}) = \text{sign}(\phi(\mathbf{x})) - \text{sign}(\phi_I), \quad I \in N_{\text{enr}} \quad \text{in } \Omega_{\text{enr}} \tag{6}$$

where $\phi_I = \phi(\mathbf{x}_I)$. Note that the sign function is shifted by $\text{sign}(\phi_I)$. Otherwise the enrichment displacement field does not vanish outside the enriched element. This shift does not alter the approximating basis but it simplifies the implementation because the resulting enrichment vanishes in all elements not cut by the crack; Figure 3 illustrates the effect of the shift in one dimension.

In the following, we consider only triangular elements. Therefore we can express all variables as functions of the area (triangular; barycentric) co-ordinates $\boldsymbol{\xi} = (\xi_1, \xi_2, \xi_3)$. The spatial

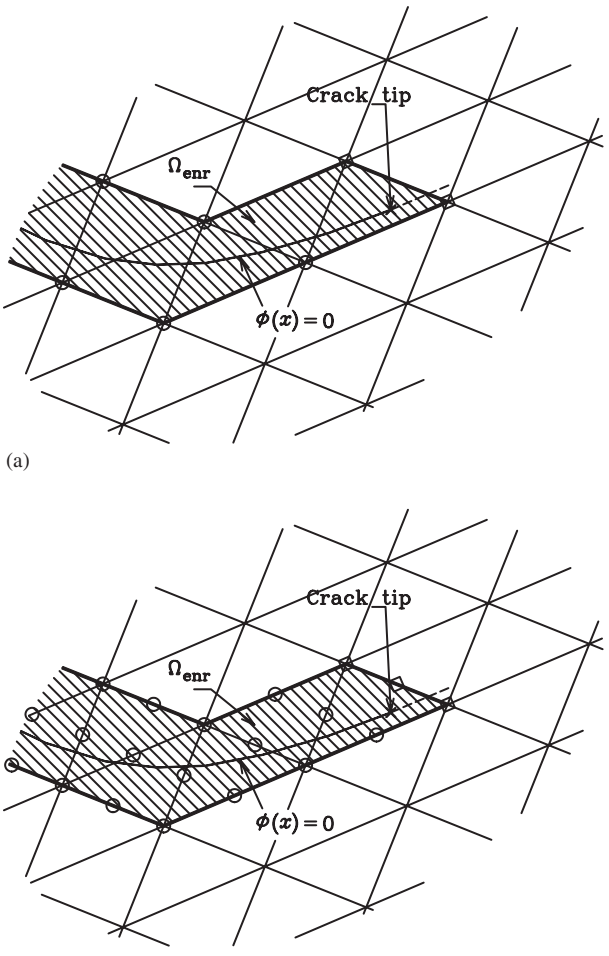

Figure 2. The enriched domain Ω_{enr} (shaded area) and the enriched nodes N_{enr} (circles), where a virtual (dashed) line segment is added to calculate the signed distance function in the tip element; at square nodes, the enrichment parameters $\mathbf{a}_I = 0$: (a) 3-node linear elements; and (b) 6-node quadratic elements.

co-ordinates are then given by

$$\mathbf{x} = \sum_{I=1}^{n_e} \mathbf{x}_I \mathbf{N}_I(\boldsymbol{\xi}) \tag{7}$$

where n_e is the number of nodes in the element.

For elements containing a crack tip, we consider first a 3-node linear element as shown in Figure 4(a) and 4(b). We consider an element with nodes 1, 2, 3 and the crack passing through side $\overline{23}$. The crack is assumed to be straight within the element. Let the direction of the crack be such that it intersects side $\overline{12}$. Other relationships between the element and the crack can be obtained by permuting the node numbers. We wish to construct an enrichment

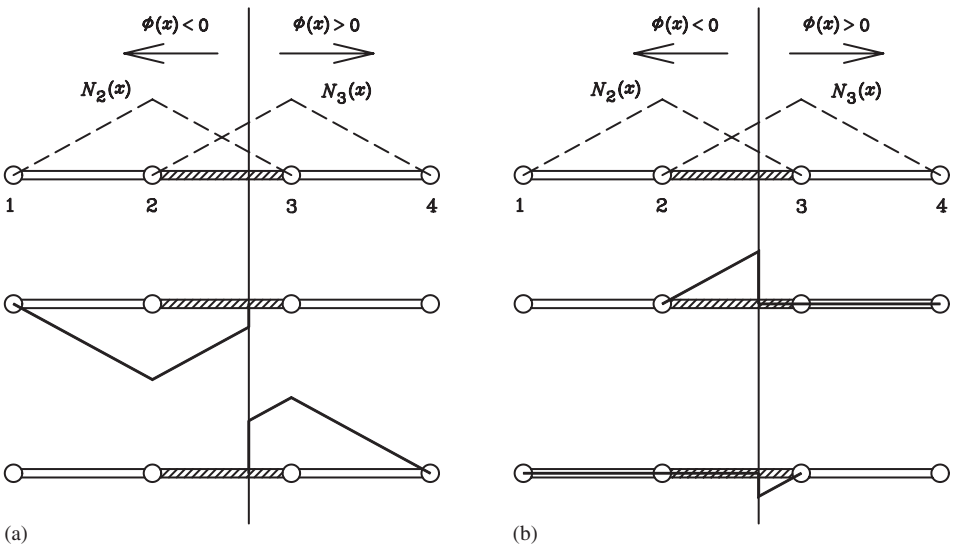

Figure 3. One-dimensional enrichment displacement fields: (a) $N_I(x)\,\mathrm{sign}(x)$; and (b) $N_I(x)\ \{\mathrm{sign}(x) - \mathrm{sign}(x_I)\}$; the regular shape functions are represented by the dashed lines and the enrichment displacement fields by the thick solid lines; the shaded elements are the enriched elements.

that vanishes on the two edges $\overline{12}$ and $\overline{13}$ (which is necessary for compatibility), and is continuous across edge $\overline{23}$ with the field in the adjacent element. To meet these conditions, only node 3 is enriched and the discontinuous displacement field in the tip element is

$$\mathbf{u}_{\mathrm{disc}} = \boldsymbol{\xi}_3^* \Psi_3(\boldsymbol{\xi}^*)\mathbf{a}_3 \tag{8}$$

where $\boldsymbol{\xi}^* = \xi_I^* = \{\xi_1^*, \xi_2^*, \xi_3^*\}$ are the parent coordinates of the shaded region 23P in Figure 4(b), i.e. the element generated by side $\overline{23}$, side $\overline{3P}$ and $\overline{P2}$, where P is the intersection point of the line joining node 2 to the crack tip and side $\overline{31}$. The shaded parent area coordinates are related by $\xi_3^* = 1 - \xi_1^* - \xi_2^*$ and $\Psi_3(\boldsymbol{\xi}^*) = \mathrm{sign}(\phi(\boldsymbol{\xi}^*)) - \mathrm{sign}(\phi_3)$. The relation between $\boldsymbol{\xi}^*$ and $\boldsymbol{\xi}$ is given by

$$\xi_1^* = \frac{\xi_1}{\xi_{1\mathrm{P}}}, \quad \xi_2^* = \xi_2 \tag{9}$$

where $\xi_{1\mathrm{P}}$ is the area co-ordinate of point P.

When the direction of the crack intersects side $\overline{31}$ (Figure 4(c) and 4(d)), then the discontinuous part of the displacement field is

$$\mathbf{u}_{\mathrm{disc}} = \boldsymbol{\xi}_2^* \Psi_2(\boldsymbol{\xi}^*)\,\mathbf{a}_2 \tag{10}$$

where

$$\xi_1^* = \xi_1 - \frac{\xi_{1\mathrm{P}}}{\xi_{2\mathrm{P}}}\,\xi_2 \quad \text{and} \quad \xi_2^* = \frac{\xi_2}{\xi_{2\mathrm{P}}} \tag{11}$$

Here, $\Psi_2(\boldsymbol{\xi}^*) = \mathrm{sign}(\phi(\boldsymbol{\xi}^*)) - \mathrm{sign}(\phi_2)$ and $\mathbf{a}_3 = \mathbf{a}_{\mathrm{P}} = 0$.

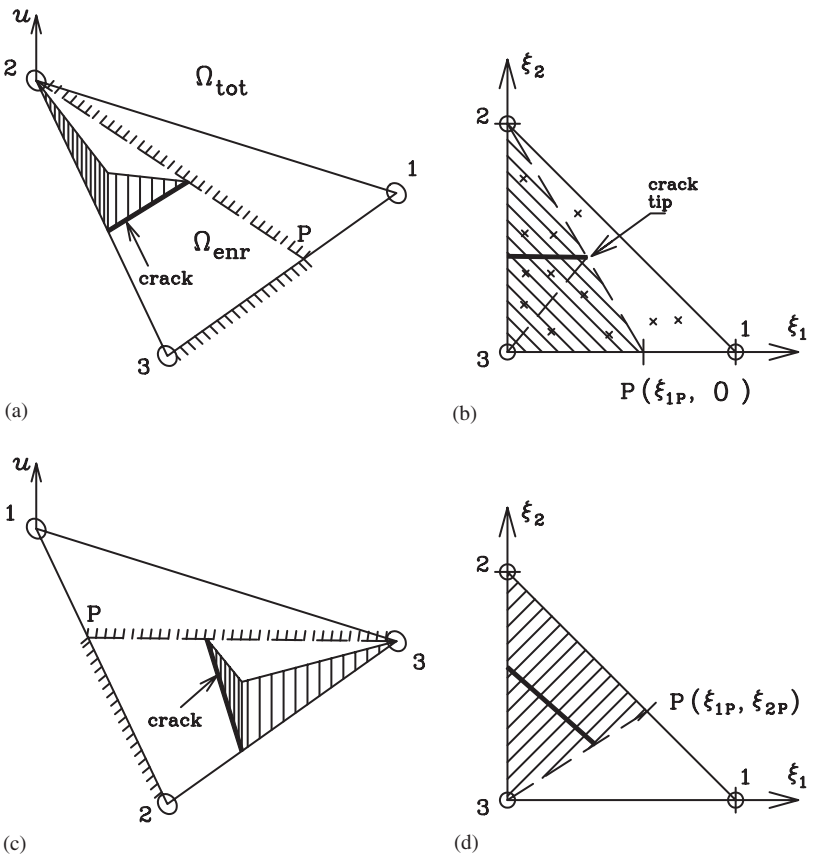

Figure 4. (a,c) Enrichment displacement field $\mathbf{u}_{\text{disc}}$, (which vanishes along $\overline{2P}$ and $\overline{3P}$, respectively), in a 3-node linear tip element and (b, d) the parent domain of the linear tip element, (in which the shaded areas represent the enriched region Ω_{enr}); crosses in (b) designate the quadrature points.

The enrichment can be implemented more easily by letting

$$\mathbf{u}_{\text{disc}} = \sum_I \xi_I^* \Psi_I(\boldsymbol{\xi}^*)\, \mathbf{a}_I \tag{12}$$

and constraining $\mathbf{a}_I$ to vanish for the nodes on the edge toward which the crack is heading, as shown in Figure 2(a).

These enrichment displacements, Equations (5), (8) and (10), vanish on the boundary of Ω_{enr} (see Figure 3(b) for the one-dimensional example). Therefore, only the elements in Ω_{enr} need a special treatment to model the crack. Furthermore, all of the elements in Ω_{enr} have enrichments of the same type. Therefore, in contrast to previous methods [2, 21], this is a partition of unity in Ω_{enr} and there is no inner blending between different enrichments. In addition, since the enrichment vanishes on the boundaries of Ω_{enr}, blending to outside the enriched subdomain does not occur. Thus, although this is a local partition of unity, it is indistinguishable from a global partition of unity.

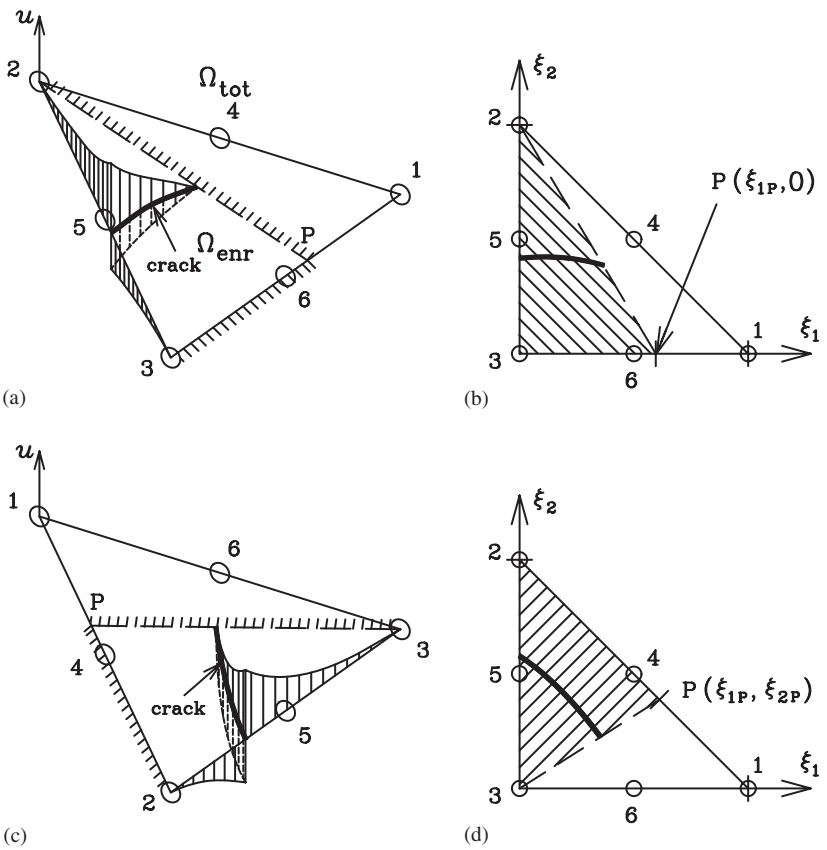

Figure 5. Enrichment displacement field $\mathbf{u}_{\text{disc}}$ in a 6-node quadratic tip element for two crack directions (a and c, respectively) and the corresponding parent domains (b and d, respectively); the shaded areas represent the enriched region Ω_{enr}.

The enrichment developed for a 3-node element is generalized to a 6-node element as follows (Figure 5). Again, let the crack cut the edge $\overline{23}$ when passing into the element. The mapping for a 6-node element is exactly the same as before, i.e. (9) and (11). The crack may be curved within the element and its direction is given in the element by a quadratic implicit function,

$$\sum_{I=1}^{6} N_I(\xi)\phi_I = 0 \tag{13}$$

where N_I are the quadratic shape functions for a 6-node triangle.

The enrichment displacement field for the case shown in Figure 5(a) and 5(b) is given by

$$\mathbf{u}_{\text{disc}} = N_3(\xi^*)\Psi_3(\xi^*)\mathbf{a}_3 + N_5(\xi^*)\Psi_5(\xi^*)\mathbf{a}_5 + N_6(\xi^*)\Psi_6(\xi^*)\mathbf{a}_6 \tag{14}$$

For the case shown in Figure 5(c) and (d)

$$\mathbf{u}_{\text{disc}} = N_2(\xi^*)\Psi_2(\xi^*)\mathbf{a}_2 + N_4(\xi^*)\Psi_4(\xi^*)\mathbf{a}_4 + N_5(\xi^*)\Psi_5(\xi^*)\mathbf{a}_5 \tag{15}$$

Based on the preceding, we can write the discontinuous displacement of a quadratic tip element as

$$\mathbf{u}_{\text{disc}} = \sum_{I \in N_{\text{enr, tip}}} N_I(\xi^*)\Psi_I(\xi)\mathbf{a}_I \tag{16}$$

with $\mathbf{a}_I = 0$ at three of the nodes as shown in Figure 2(b).

3. SIGNED DISTANCE FUNCTION

The choice of the sign of the signed distance function ϕ does not change the computational results. When the sign of ϕ is altered, the sign of the enrichment parameters $\mathbf{a}_I$ change sign. Therefore, the sign of ϕ can be chosen arbitrarily as long as the sign is consistent along the crack Γ_c.

The absolute value of the signed distance function at a point $\mathbf{x}$ is defined as the minimum distance to the crack Γ_c. Given the nodal values of the signed distance function ϕ_I, the signed distance function at any point in the enriched domain Ω_{enr} can be interpolated by means of finite element shape functions;

$$\phi(\mathbf{x}) = \sum_{I \in N_{\text{enr}}} N_I(\mathbf{x})\phi_I \tag{17}$$

The unit normal $\mathbf{n}$ (Figure 1) in the positive direction is easily determined by

$$\mathbf{n} = \frac{\partial \phi}{\partial \mathbf{x}} \tag{18}$$

Although other interpolation techniques, such as the moving least squares [27], are available, (17) is the simplest yet accurate enough to capture the crack growth. Methods for updating the level set are given in Ventura *et al.* [28, 29].

4. VARIATIONAL PRINCIPLE OF XFEM AND DISCRETIZED EQUATIONS

The weak form of equilibrium is given by

$$\delta W^{\text{int}} = \delta W^{\text{ext}} + \delta W^{\text{coh}} \tag{19}$$

where

$$\delta W^{\text{int}} = \int_{\Omega} \frac{\partial \delta \mathbf{u}}{\partial \mathbf{x}} : \boldsymbol{\sigma} \, \mathrm{d}\Omega \tag{20}$$

$$\delta W^{\text{ext}} = \lambda \int_{\Gamma_t} \delta \mathbf{u} \cdot \boldsymbol{\tau}_0 \, \mathrm{d}\Gamma \tag{21}$$

$$\delta W^{\mathrm{coh}} = \int_{\Gamma_{c^+}} \delta \mathbf{u}^+ \cdot \boldsymbol{\tau}^{c+} \mathrm{d}\Gamma + \int_{\Gamma_{c^-}} \delta \mathbf{u}^- \cdot \boldsymbol{\tau}^{c-} \, \mathrm{d}\Gamma \tag{22}$$

$$= - \int_{\Gamma_c} \tau^c \mathbf{n} \cdot \delta(\mathbf{u}^+ - \mathbf{u}^-) \, \mathrm{d}\Gamma \tag{23}$$

Here W^{int} is the internal work, W^{ext} is the external work of the traction $\lambda \boldsymbol{\tau}_0$ along the traction boundary Γ_t, W^{coh} is the work by cohesive traction along cohesive crack Γ_c, λ is the load factor, $\boldsymbol{\tau}_0$ is the normalized external traction on Γ_t, $\delta \mathbf{u}$ is the test function (which vanishes along the displacement boundary Γ_u), $\boldsymbol{\sigma}$ is the stress, $\boldsymbol{\tau}^c = \tau^c(w)\mathbf{n}$ is the cohesive traction along the cohesive crack Γ_c, $\tau^c(w)$ is a softening law, w is the crack opening displacement. It is assumed that the direction of the cohesive traction $\boldsymbol{\tau}^c$ coincides with the normal direction $\mathbf{n}$ of the crack line Γ_c. The crack opening displacement w is given by

$$w = \mathbf{n} \cdot (\mathbf{u}^+ - \mathbf{u}^-) = \mathbf{n} \cdot 2 \sum_{I \in N_{\mathrm{enr}}} N_I \mathbf{a}_I \tag{24}$$

From the weak form (19) and the enrichment displacement field (3)–(5) or (3), (4), (16), one can obtain the discrete equilibrium equation:

$$\mathbf{f}^{\mathrm{int}} = \mathbf{f}^{\mathrm{ext}} + \mathbf{f}^{\mathrm{coh}} \tag{25}$$

where

$$\mathbf{f}^{\mathrm{int}} = \mathbf{K} \cdot \mathbf{q} = \int_\Omega \mathbf{B}^{\mathrm{T}} \mathbf{C} \mathbf{B} \, \mathrm{d}\Omega \cdot \mathbf{q} \tag{26}$$

$$\mathbf{f}^{\mathrm{ext}} = \lambda \int_{\Gamma_t} \mathbf{N}^{\mathrm{T}} \boldsymbol{\tau}_0 \, \mathrm{d}\Gamma \tag{27}$$

$$\mathbf{f}^{\mathrm{coh}} = -2 \int_{\Gamma_c} \tau^c(w) \mathbf{N}^{\mathrm{T}} \mathbf{n} \, \mathrm{d}\Gamma \tag{28}$$

Here $\mathbf{f}^{\mathrm{int}}$, $\mathbf{f}^{\mathrm{ext}}$ and $\mathbf{f}^{\mathrm{coh}}$ are the internal, external and cohesive forces, respectively. $\mathbf{K}$ is the stiffness matrix, $\mathbf{q} = [\mathbf{q}_1^{\mathrm{T}}, \mathbf{q}_2^{\mathrm{T}}, \ldots, \mathbf{q}_{N_{\mathrm{tot}}}^{\mathrm{T}}]^{\mathrm{T}}$, $\mathbf{q}_I = [\mathbf{u}_I^{\mathrm{T}}, \mathbf{a}_I^{\mathrm{T}}]^{\mathrm{T}}$ are the generalized nodal displacements, $\mathbf{B}$ is the strain–displacement matrix and $\mathbf{C}$ is the tangential modulus matrix. The $\mathbf{B}$ matrix is given by

$$\mathbf{B} = \begin{Bmatrix} \mathbf{B}^0 & \text{for unenriched elements and} \\ [\mathbf{B}^0 \quad \mathbf{B}^{\mathrm{e}}] & \text{for enriched elements} \end{Bmatrix} \tag{29}$$

where $\mathbf{B}^0$, $\mathbf{B}^{\mathrm{e}}$ are the regular and the enriched parts, respectively. The $\mathbf{B}^0$ and $\mathbf{B}^e$ matrices are given by

$$\mathbf{B}^0 = [\mathbf{B}_1^0, \ \mathbf{B}_2^0, \ldots, \mathbf{B}_{n_e}^0] \quad \text{and} \quad \mathbf{B}^{\mathrm{e}} = [\mathbf{B}_1^{\mathrm{e}}, \ \mathbf{B}_2^{\mathrm{e}}, \ldots, \mathbf{B}_{n_e}^{\mathrm{e}}] \tag{30}$$

$$\mathbf{B}_I^0 = \begin{bmatrix} N_{I,x} & 0 \\ 0 & N_{I,y} \\ N_{I,y} & N_{I,x} \end{bmatrix} \quad \text{and} \quad \mathbf{B}_I^{\mathrm{e}} = \begin{bmatrix} N_{I,x}\Psi_I & 0 \\ 0 & N_{I,y}\Psi_I \\ N_{I,y}\Psi_I & N_{I,x}\Psi_I \end{bmatrix} \tag{31}$$

$$\nabla N_I = \begin{cases} \left[\dfrac{\partial N_I}{\partial \boldsymbol{\xi}} \cdot \left(\dfrac{\partial \mathbf{x}}{\partial \boldsymbol{\xi}} \right)^{-1} \right] & \text{for the regular and the completely cut elements} \\ \left[\dfrac{\partial N_I}{\partial \boldsymbol{\xi}} \cdot \dfrac{\partial \boldsymbol{\xi}^*}{\partial \boldsymbol{\xi}} \cdot \left(\dfrac{\partial \mathbf{x}}{\partial \boldsymbol{\xi}} \right)^{-1} \right] & \text{for the tip element} \end{cases} \tag{32}$$

The derivative of the enrichment function Ψ does not appear in (32) because the domain Ω is defined to be an open set that does not include the crack Γ_c and the derivative of the enrichment function $\partial\Psi/\partial\mathbf{x}$ vanishes in Ω.

5. THE CONDITION FOR SMOOTH CRACK CLOSING AND THE DIRECTION OF CRACK GROWTH

In addition to the equilibrium condition (25), one more condition is needed to obtain the load factor λ in (27). By the definition of the cohesive crack model [17], the stress intensity factor at the crack tip should vanish, which implies that the crack closes smoothly. This condition is called the zero stress intensity factor condition. Because the mode II stress intensity factor is typically negligible compared to the mode I stress intensity factor, only the mode I stress intensity factor is taken into account [21], i.e.

$$\mathbf{K}_{I_{\text{tip}}} = 0 \tag{33}$$

where $\mathbf{K}_{I_{\text{tip}}}$ is the mode I stress intensity factor calculated at the crack tip. In the finite element method, the stress intensity factor at the crack tip is efficiently calculated by means of the domain integration technique [30] (also see Reference [21]).

Alternatively, and equivalent in principle, one may require the stress projection in the normal direction $\mathbf{n}$ of the crack to be equal to the tensile strength of the material, since the zero stress intensity factor implies that the stress at the tip should be finite [19, 20, 24, 31, 32], i.e.

$$\mathbf{n} \cdot \boldsymbol{\sigma} \cdot \mathbf{n} = f_{\text{t}} \tag{34}$$

where $\boldsymbol{\sigma}$ is the stress at the crack tip and f_{t} is the tensile strength of material. This condition will be referred to as the stress condition in the following. Either (33) or (34) could be used but the stress condition (34) is simpler and will be used here.

The direction of crack growth is determined by using the stress intensity factors [21,23, 33,34], so

$$\theta = 2 \arctan \frac{1}{4} \left(\rho_K^{\text{ext}} \pm \sqrt{\rho_K^{\text{ext}^2} + 8} \right) \tag{35}$$

where $\rho_K^{\text{ext}} = K_{\text{I}}^{\text{ext}} / K_{\text{II}}^{\text{ext}}$ is the ratio of external mode I and mode II stress intensity factors and θ represents the direction of the crack growth relative to the tangent to crack at the tip.

6. ALGORITHM

The solution should simultaneously satisfy the equilibrium condition (25) and the stress condition (34). This stress condition (34) can be written as

$$\mathbf{S} \cdot \mathbf{q}_I^e = f_t \tag{36}$$

where $\mathbf{S} = \mathbf{M}^T \cdot \mathbf{C} \cdot \mathbf{B}$ is an operator by which stress at the tip is calculated, $\mathbf{M} = \mathbf{n} \otimes \mathbf{n}$ in Voigt notation and $\mathbf{q}_I^e$ are the generalized nodal displacements of element e.

Using (25) and (34), we solve for $\mathbf{q}$ and λ directly by means of the Newton–Raphson method. The residual of the Newton–Raphson method is given by

$$\mathbf{r} = \begin{Bmatrix} \mathbf{K} \cdot \mathbf{q} - \mathbf{f}^{ext}\lambda - \mathbf{f}^{coh}(\mathbf{q}) \\ f_t - \mathbf{S}\mathbf{q} \end{Bmatrix} \tag{37}$$

where the independent variables of the Newton–Raphson method are $\mathbf{q}$ and λ. The Jacobian is

$$\mathbf{A} = \begin{bmatrix} \mathbf{K} - \dfrac{\partial \mathbf{f}^{coh}(\mathbf{q})}{\partial \mathbf{q}} & -\mathbf{f}^{ext} \\ -\mathbf{S} & 0 \end{bmatrix} \tag{38}$$

where

$$\frac{\partial \mathbf{f}^{coh}(\mathbf{q})}{\partial \mathbf{q}} = -2 \int_{\Gamma_c} \frac{\partial \tau^c(w)}{\partial w} \mathbf{N}^T \cdot \mathbf{n} \cdot \mathbf{n}^T \cdot \mathbf{N} \, d\Gamma \tag{39}$$

From Equations (37) and (38), the increments of the independent variables at the ith iteration are

$$\begin{Bmatrix} \Delta \mathbf{q} \\ \Delta \lambda \end{Bmatrix}^i = -\left(\mathbf{A}^{i-1}\right)^{-1} \cdot \mathbf{r}^{i-1} \tag{40}$$

The overall algorithm is as follows:

1. Calculate the signed distance function for a given crack.
2. Construct the stiffness matrix $\mathbf{K}$ using (26).
3. Calculate the derivative of the cohesive force with respect to the generalized nodal displacements using (39).
4. Calculate the Jacobian of the Newton–Raphson method, (38), the residual (37) and the increments (40).
5. Iterate step 4 until $\mathbf{q}$ and λ converge.
6. Calculate the direction of crack growth (35) and grow the crack in that direction.
7. Go to step 1.

In the first step, the fracture process zone is not developed yet. Therefore, λ is simply obtained from the condition that the stress at the notch tip should be equal to the strength f_t.

7. NUMERICAL STUDY

7.1. Example

In order to study the new XFEM scheme, we solved the double-cantilever-beam (DCB) problem shown in Figure 6(a); a linear softening law (Figure 6(b)) is used. Young's modulus is 36.5 GPa and Poisson's ratio is 0.18. The results obtained by the new XFEM scheme are compared to those obtained by the static condensation method [20] which has extensively been used to analyze the fracture properties of many experimental tests when the direction of crack propagation is known [18–20, 31, 35]. The static condensation method is also known as the pseudo boundary integral (PBI) method.

Because the crack propagation path in the static condensation method must be predetermined, the angle θ in (35) is fixed to zero to make the crack propagate in a straight line. To save computation time, only the elements along the anticipated crack path are refined; they are as small as 0.82 mm (Figure 7). The crack passes through the elements in the mesh as shown in Figure 7(a). The mesh for the static condensation method is shown in Figure 7(b) which corresponds to half of the DCB specimen because of symmetry.

To examine how the choice of the cohesive crack criteria (33) or (34) affects the results, two cases are considered; (i) the zero stress intensity factor condition Equation (33) and (ii) the stress condition at the tip Equation (34). Because it is not easy to obtain the Jacobian matrix for the Newton–Raphson method when the zero stress intensity factor condition is used, in the first case, the secant method is used to obtain the load factor λ iteratively; the displacement $\mathbf{u}$ corresponding to a value of λ is obtained by the Newton–Raphson method.

7.2. Convergence rate and load–deflection history

Because no analytical solution of the problem is available, the load–deflection histories with the most refined mesh are chosen as the reference solution. The error is defined as the ratio of the area between a reference curve and the current curve to the total area under the

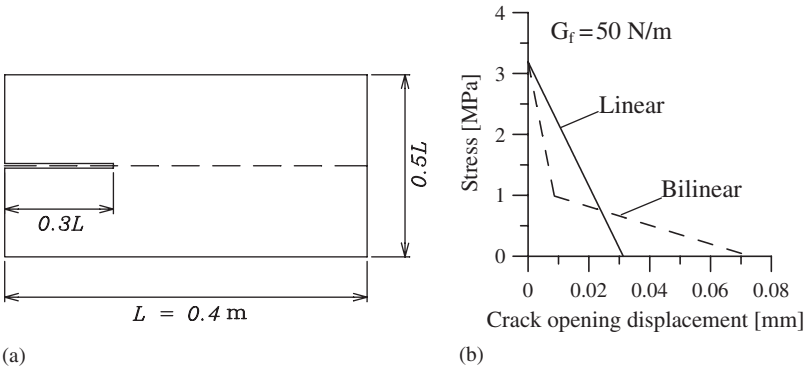

Figure 6. (a) A double-cantilever-beam (DCB) with 30% notch; and (b) softening traction-displacement laws; the solid line represents a linear softening law and the dashed line represents a bilinear softening law; the crack opening and stresses σ_y are measured along the dashed line in (a).

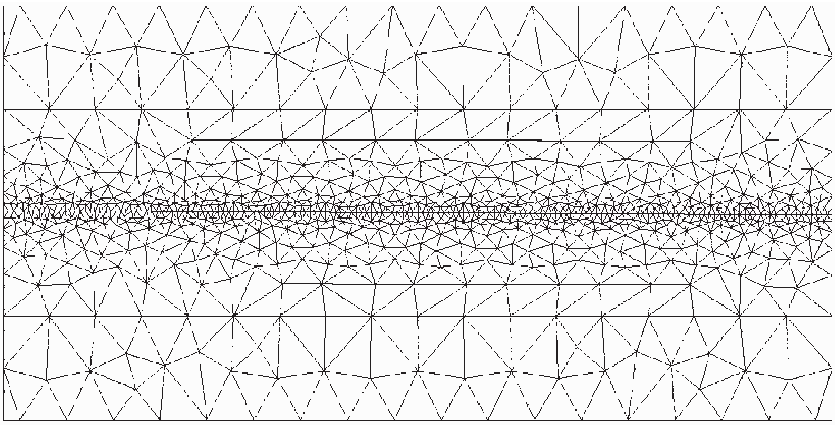

(a)

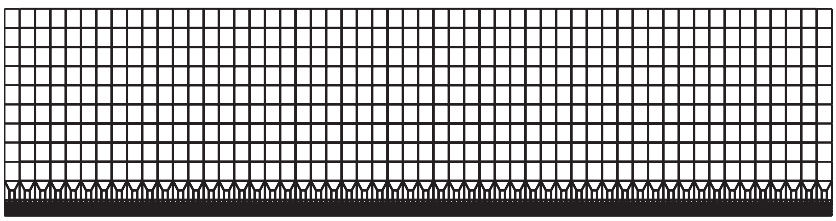

(b)

Figure 7. (a) A mesh which consists of 6-node triangular elements used for the extended finite element method, in which $h_{\min} \sim 1.8$ mm; and (b) a mesh which consists of 4-node quadrilateral elements used for the static condensation method, in which $h_{\min} \sim 0.82$ mm and only a half of the specimen is modelled because of the symmetry of the DCB specimen.

reference curve:

$$\text{error} = \frac{\int_0^u |f^{\text{comp}} - f^{\text{ref}}| \, \mathrm{d}\bar{u}}{\int_0^u |f^{\text{ref}}| \, \mathrm{d}\bar{u}} \tag{41}$$

where u is the load–point displacement, and f^{comp} and f^{ref} are the computed load–deflection curve and the reference one, respectively. The convergence rates for the linear and quadratic elements for various mesh refinements are shown in Figure 8. The convergence rate of the second-order method, 1.23, is much better than the first-order method, 0.48, respectively.

The load–deflection histories for the quadratic elements with the stress condition are plotted and compared to the result by the static condensation method in Figure 9. The load–deflection histories are calculated for three different mean refinements and, for all cases, agree well with the reference.

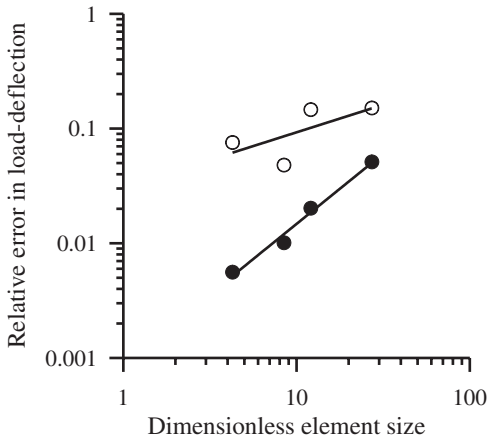

Figure 8. Relative errors in load–deflection histories obtained by the extended finite element methods with linear displacement triangles (empty circles) and quadratic displacement triangles (solid symbols).

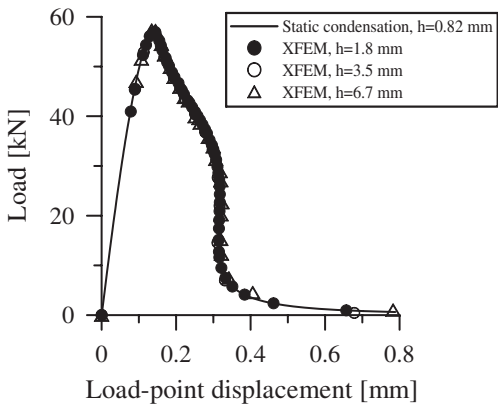

Figure 9. Load–deflection histories obtained by the second order XFEM scheme with the stress condition (34), in which the linear softening law in Figure 6(b) is used for every case.

7.3. Crack opening and stress profiles

The crack opening is shown in Figure 10 and the stresses σ_y are shown in Figure 11 for three different mesh refinements: $h = 2, 5$ and 11 mm. They are scaled by the critical crack opening displacement w_c and the tensile strength f_t, respectively. Because the enrichment function is based on a partition of unity, spurious crack opening is not observed even in the coarse mesh. The crack opening profiles for $h = 2$ mm almost coincide with the reference crack opening profiles so that the difference is indiscernible.

The stresses on the dashed line in Figure 6(a) are plotted in Figure 11. It can be seen that the change of the stress profiles as the crack advances in the fracture process zone is

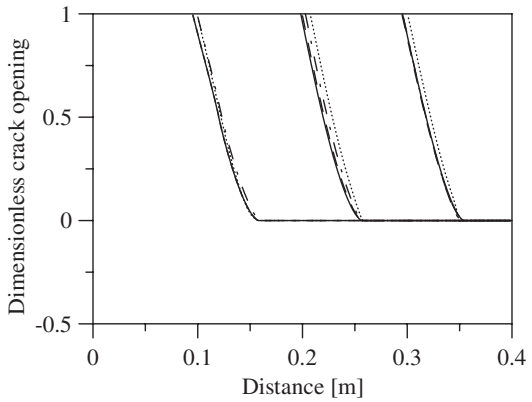

Figure 10. Comparison of dimensionless crack opening profiles by the extended finite element method (dashed line: $h = 2$ mm, dash-dot line: $h = 5$ mm, dotted line: $h = 11$ mm) and the static condensation method (solid lines); the crack openings are scaled by the critical opening w_c.

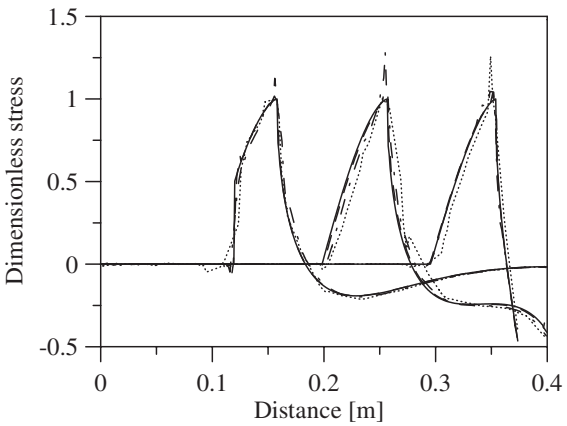

Figure 11. Comparison of dimensionless stresses σ_y by the extended finite element method (dashed line: $h = 2$ mm, dash-dot line $h = 5$ mm, dotted line: $h = 11$ mm) and the static condensation method (solid lines); the stresses are scaled by the material strength f_t.

approximately self-similar. As the mesh is refined, the stress profiles converge to the reference profiles. The stress profiles for $h = 2$ mm agree well with the reference profiles.

7.4. Bilinear softening law

Because of their simplicity, linear softening laws are frequently used. However, when post-peak behaviour is important, non-linear softening laws may be more accurate. Equations (37) and (38) can be applied to non-linear softening laws as well as linear softening laws.

One might think that if the fracture energy of two different softening laws is identical, the load–deflection curve does not change. But, it has been shown analytically by Bažant

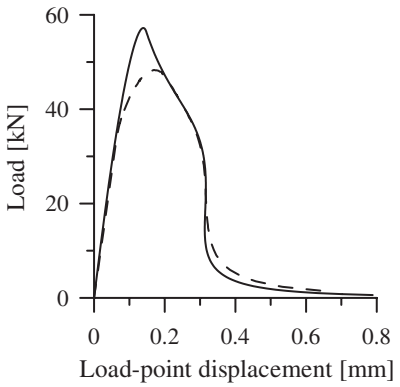

Figure 12. Comparison of the load–deflection histories in the cases where the linear softening law (solid line) and the bilinear softening law (dashed line) are used, respectively.

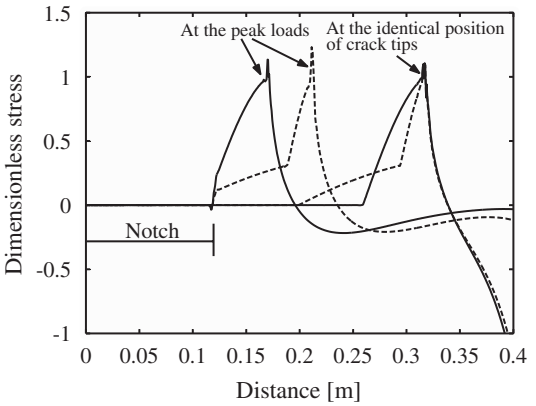

Figure 13. Dimensionless stresses σ_y at the peak load for the linear softening law (solid line) and the bilinear softening law (dashed line), respectively.

and Zi [36] that the nominal strength of a structure is affected by the shape of softening laws.

A bilinear softening law is shown in Figure 6(b). The tensile strength and the fracture energy of the bilinear softening law (dashed line) are the same as those of the linear softening law (solid line). The load–deflection histories for the two are compared in Figure 12. The peak load associated with the bilinear softening law is smaller than the linear one and the shapes of the load–deflection histories differ as well. As one can see in Figure 13, the fracture process zones are not fully developed at the peak loads, to which only the initial parts of the softening curves (in Figure 6(b)) contribute. Therefore the fracture energies associated with the peak loads are different although the fracture energies for the two softening laws are the same.

7.5. Simulation of curved crack growth

We consider a problem of curved cohesive crack growth. This problem has been considered by Belytschko *et al.* [1] with EFG, and involves an instability in the crack path which curves the crack. To trigger this instability, the notch of the DCB specimen is placed 2 mm (2%) off the centre line. The paths of the cracks for various mesh refinements are shown in Figure 14(a) and the load–deflection histories are depicted in Figure 14(b).

Because the position of the new crack tip is calculated based on the stress intensity factors of the current configuration, the paths do not coincide but they agree better as the mesh is refined. The crack paths do not converge uniformly. For moderate refinement ($h = 3.3\,\text{mm}$) the path shifts forward and then returns to an intermediate path with further refinement. The crack path turns back near the boundary of the specimen. This happens because the calculation of the stress intensity factors that drive the direction of crack growth by (35) is not accurate near the boundary.

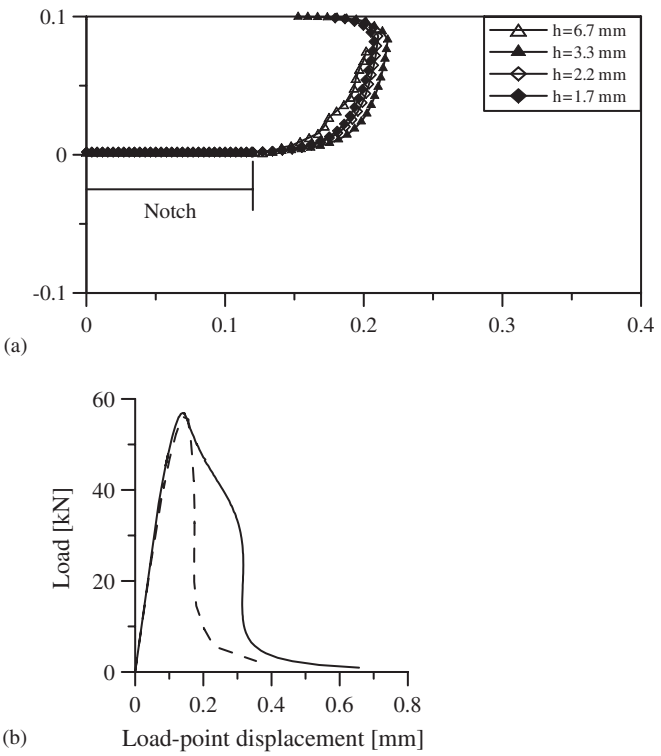

Figure 14. (a) The crack growing paths of the DCB specimen for various mesh refinements; and (b) the change of the load–deflection when the crack path is curved; straight crack (solidline) and curved crack (dashed line).

8. CONCLUSIONS

A new XFEM scheme for static cohesive cracks has been developed in the framework of the extended finite element method. All the cracked elements, including the tip element, are enriched by the sign function so that the partition of unity holds in the entire domain. The parent domain of the partially cracked tip element is divided into two parts: the cracked and the uncracked parts. Only the cracked part is enriched by the sign function. That scheme is applied to the linear 3-node and the quadratic 6-node elements. Although the branch function is not used in the scheme developed in this paper, the crack tip can be located anywhere inside the tip element. The path of the crack can be completely independent of mesh.

ACKNOWLEDGEMENTS

The support of the Office of Naval Research and the Department of Energy are acknowledged.

REFERENCES

1. Belytschko T, Krongauz Y, Organ D, Fleming M, Krysl P. Meshless methods: an overview and recent developments. *Computer Methods in Applied Mechanics and Engineering* 1996; **139**:3–47.
2. Belytschko T, Black T. Elastic crack growth in finite elements with minimal remeshing. *International Journal for Numerical Methods in Engineering* 1999; **45**(5):601–620.
3. Melenk JM, Babuška I. The partition of unity finite element method: basic theory and application. *Computer Methods in Applied Mechanics and Engineering* 1996; **139**:289–314.
4. Chessa J, Wang H, Belytschko T. On the construction of blending elements for local partition of unity enriched finite elements. *International Journal for Numerical Methods in Engineering* 2003; **57**(7):1015–1038.
5. Moës N, Dolbow J, Belytschko T. A finite element method for crack growth without remeshing. *International Journal for Numerical Methods in Engineering* 1999; **46**(1):131–150.
6. Dolbow J, Moës N, Belytschko T. Discontinuous enrichment in finite elements with a partition of unity method. *Finite Elements in Analysis and Design* 2000; **36**(3):235–260.
7. Dolbow J, Moës N, Belytschko T. An extended finite element method for modeling crack growth with friction contact. *Computer Methods in Applied Mechanics and Engineering*, 2000, in press.
8. Daux C, Moës N, Dolbow J, Sukumar N, Belytschko T. Arbitrary branched and intersecting cracks with the extended finite element method. *International Journal for Numerical Methods in Engineering* 2000; **48**: 1741–1760.
9. Sukumar N, Moës N, Moran B, Belytschko T. Extended finite element method for three-dimensional crack modeling. *International Journal for Numerical Methods in Engineering* 2000; **48**(11):1549–1570.
10. Belytschko T, Moës N, Usui S, Parimi C. Arbitrary discontinuities in finite elements. *International Journal for Numerical Methods in Engineering* 2001; **50**(4):993–1013.
11. Sukumar N, Chopp DL, Moës N, Belytschko T. Modeling holes and inclusions by level sets in the extended finite element method. *Computer Methods in Applied Mechanics and Engineering* 2000; **190**(46–47): 6183–6200.
12. Chessa J, Belytschko T. An extended finite element method for two-phase fluids. *Journal of Applied Mechanics* (ASME) 2003; **70**(1):10–17.
13. Stazi F, Budyn E, Chessa J, Belytschko T. XFEM for fracture mechanics with quadratic elements. *Computational Mechanics* 2003; **31**(1–2):38–48.
14. Wells GN, de Borst R, Sluys LJ. A consistent geometrically non-linear approach for delamination. *International Journal for Numerical Methods in Engineering* 2002; **54**(9):1333–1355.
15. Chen H. Enriched finite element methods and its applications. *Ph.D. Thesis*, Northwestern University, 2003.
16. Dugdale DS. Yielding of steel sheets containing slits. *Journal of Mechanics and Solids* 1960; **8**:100–108.
17. Barenblatt GI. The mathematical theory of equilibrium of cracks in brittle fracture. *Advances in Applied Mechanics* 1962; **7**:55–129.
18. Petersson PE. Crack growth and development of fracture zone in plain concrete and similar materials. *Technical Report* TVBM-1006, Division of Building Materials, Lund Institute of Technology, Lund, Sweden, 1981.
19. Hillerborg A, Petersson PE, Modéer M. Analysis of crack formation and crack growth in concrete by means of fracture mechanics and finite elements. *Cement and Concrete Research* 1976; **6**:773–782.
20. Zi G, Bažant ZP. Eigenvalue method for computing size effect of cohesive cracks with residual stress, with application to kink bands in composites. *International Journal of Engineering Science* 2003, accepted.
21. Moës N, Belytschko T. Extended finite element method for cohesive crack growth. *Engineering Fracture Mechanics* 2002; **69**(7):813–833.
22. Camacho G, Ortiz M. Computational modelling of impact damage in brittle materials. *International Journal of Solids and Structures* 1996; **33**:2899–2938.
23. Bocca P, Carpinteri A, Valente S. Mixed mode fracture of concrete. *International Journal of Solids and Structures* 1991; **27**:1139–1153.
24. Carpinteri A. Post-peak and post-bifurcation analysis of cohesive crack propagation. *Engineering Fracture Mechanics* 1989; **32**:265–278.
25. Wells GN, Sluys LJ. A new method for modelling cohesive cracks using finite elements. *International Journal for Numerical Methods in Engineering* 2001; **50**(12):2667–2682.
26. Chen H, Belytschko T. Discontinuous enrichment with cohesive zone model for dynamic crack propagation. *International Journal for Numerical Methods in Engineering*, 2003.
27. Belytschko T, Lu YY, Gu L. Element-free galerkin methods. *International Journal for Numerical Methods in Engineering* 1994; **37**(2):229–256.
28. Ventura G, Budyn E, Belytschko T. Vector level set for description of propagating cracks in finite elements. *Journal of Computational Physics* 2003, in preparation.
29. Ventura G, Xu JX, Belytschko T. A vector level set method and new discontinuity approximations for crack growth by EFG. *International Journal for Numerical Methods in Engineering* 2002; **54**(6):923–944.
30. Moran B, Shih C. Crack tip and associated domain integrals from momentum and energy balance. *Engineering Fracture Mechanics* 1987; **39**:3601–3623.

31. Bažant ZP, Li YN. Stability of cohesive crack model: part II—Eigenvalue analysis of size effect on strength and ductility of structures. *Journal of Applied Mechanics* (ASME) 1995; **62**:965–969.
32. Hillerborg A. Numerical methods to simulate softening and fracture of concrete. In *Fracture Mechanics of Concrete: Structural Application and Numerical Calculation*, Sih GC, DiTomasso A (eds). Martinus Nijhoff: Dordrecht, 1985; 141–170.
33. Cendón DA, Gálvez JC, Elices M, Planas J. Modeling the fracture of concrete under mixed loading. *International Journal of Fracture* 2000; **103**:293–310.
34. Ingraffea AR, Gerstle W, Gergely P, Saouma V. Fracture mechanics in bond reinforced concrete. *Journal of the Structural Division* (ASCE) 1984; **110**(4):871–890.
35. Guinea GV, Elices M, Planas J. On the initial shape of the softening function of cohesive materials. *International Journal of Fracture* 1997; **87**:139–149.
36. Bažant ZP, Zi G. Asymptotic stress intensity factor density profiles for smeared-tip method for cohesive fracture. *International Journal of Fracture* 2003, in press.

